# Supplementary information

# A novel eutectic solvent precursor for efficiently preparing N-doped hierarchically porous carbon nanosheets with unique surface functional groups and micro-pores towards dual-carbon lithium-ion capacitors

*Kaixiang Zou,[a] Yuanfu Deng,[*a,b] Weijing Wu,[a] Shiwei Zhang,[a] and Guohua Chen[c]*

[a] The Key Laboratory of Fuel Cell for Guangdong Province, School of Chemistry and Chemical Engineering, South China University of Technology, Guangzhou, 510640, China;

[b] Electrochemical Energy Engineering Research Center of Guangdong Province, South China University of Technology, Guangzhou, 510640, China;

[c] Department of Mechanical Engineering, The Hong Kong Polytechnic University, Hung Hom, Kowloon, Hong Kong, China.

*Corresponding author. E-mail address: chyfdeng@scut.edu.cn (Y. F. Deng).

# Experimental Section

***Physical characterizations:***

Before the electric conductivities test, the slurries which contain 90 wt% of samples, and 10 wt.% of polyvinylidene fluoride (PVDF) were uniformly dispersed in N-methyl-2-pyrrolidone (NMP). Subsequently, the as-received slurries were uniformly coated on the non-conducting Celgard 2500 separator. These coated separators were applied in the electric conductivities test.

In order to ensure that the contact angle data conforms to the real situation, the prepared electrodes were adopted in the contact angle measurement. These electrodes were prepared by coating the slurries on Al foils. The slurries contain 80 wt% of active materials, 10 wt.% of acetylene black and 10 wt.% of polyvinylidene fluoride (PVDF), which are uniformly dispersed in N-methyl-2-pyrrolidone (NMP).

The thermogravimetric analysis (TGA) of the precursor is tested on a thermal analyzer (SDTQ600) under $N_2$ from 25 to 900 °C. The heating rate is set up at 5 °C $min^{-1}$. X-ray powder diffraction (XRD) was performed on a Bruker D8 ADVANCE powder diffractometer using Cu Kα radiation at 40 kV and 40 mA at a step of 0.020. The microstructures of all samples were studied with field emission scanning electron microscopy (FE-SEM, Ultra Plus, Carl Zeiss, Germany) and transmission electron microscopy (TEM, JEM-2100, Japan). The Raman spectra were obtained using a Bio-Rad FTS6000 Raman spectrophotometer with a 532 nm blue laser beam. Nitrogen absorption-desorption measurements were performed at −196 °C using an ASAP 2020 system (Micrometitics). The specific surface area (SSA) was estimated by the Barrett−Emmett−Teller (BET) method. The total volume was estimated by the Barrett-Joyner-Halenda (BJH) method. The micropore volume and pore size distribution was analyzed using the density functional theory (DFT). All samples were degassed at 180 °C for 2 h prior to sorption measurements. The elemental microanalysis (C, H, and N) and atom binding states were characterized by elemental analyzer (Vario EL) and X-ray photoelectron spectroscopy (XPS, Escalab 210, Germany), respectively.

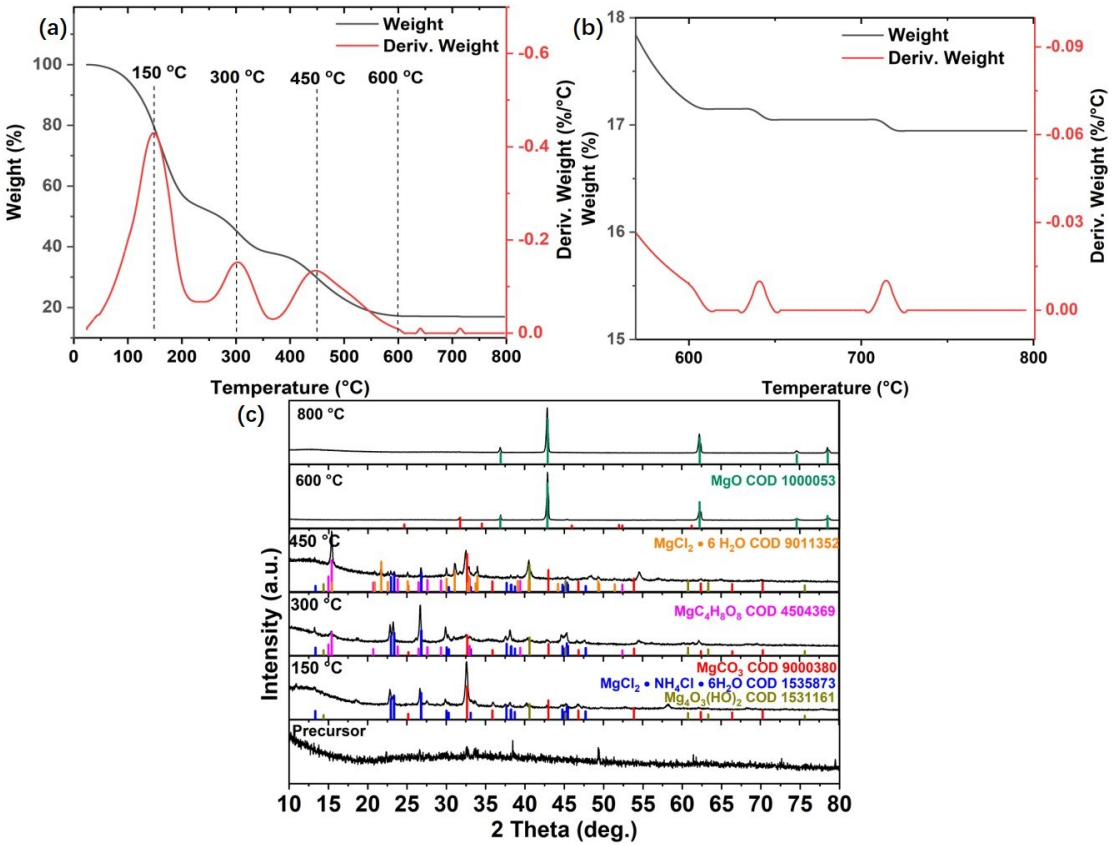


Fig. S1. (a), (b) TG curves and differential thermogravimetric curves of NPCS-1 precursor and (c) XRD pattern of the NPCS-1 precursor at different temperatures.

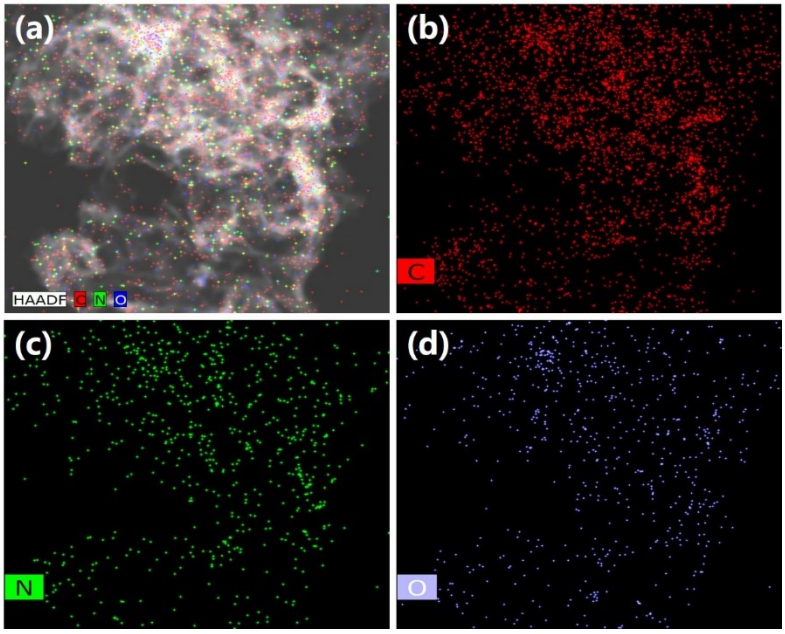


Fig. S2. HAADF image (a), C (b), N (c), and O (c) element mapping of NPCS-1.

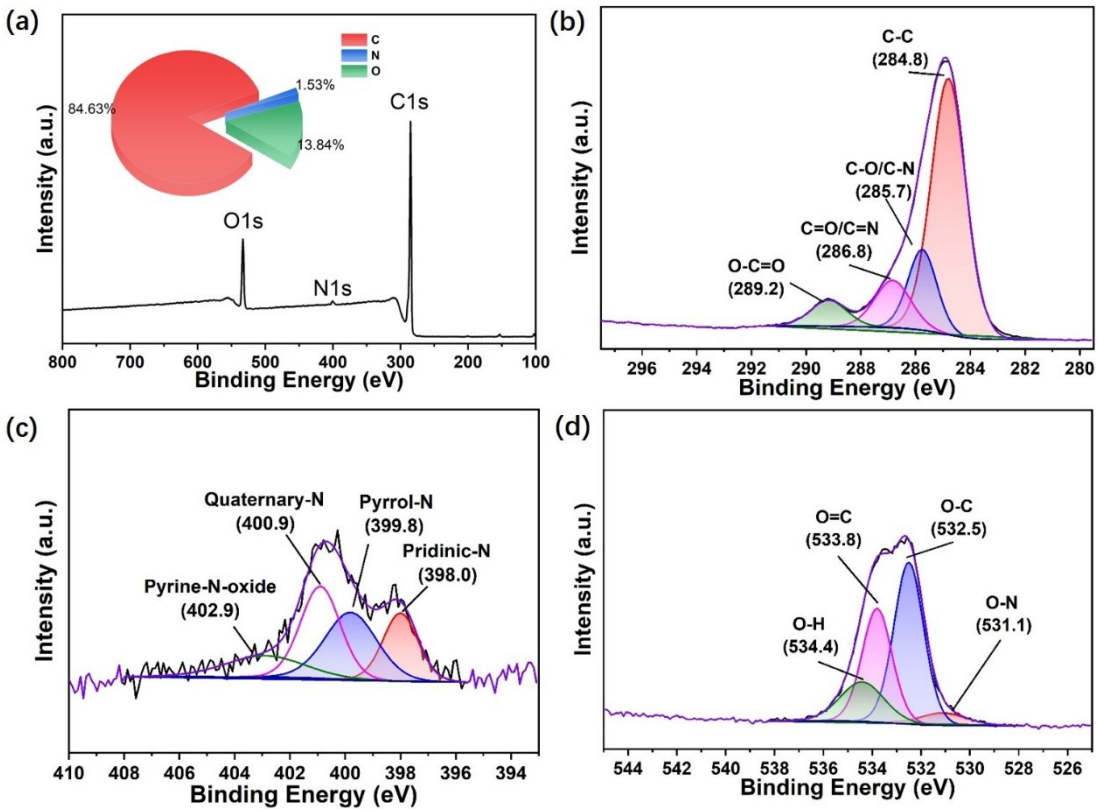


Fig. S3. (a) The XPS survey spectra, (b) high-resolution XPS C1s spectra, (c) high-resolution XPS N1s spectra, and (d) high-resolution XPS O1s spectra of NPCS-0.

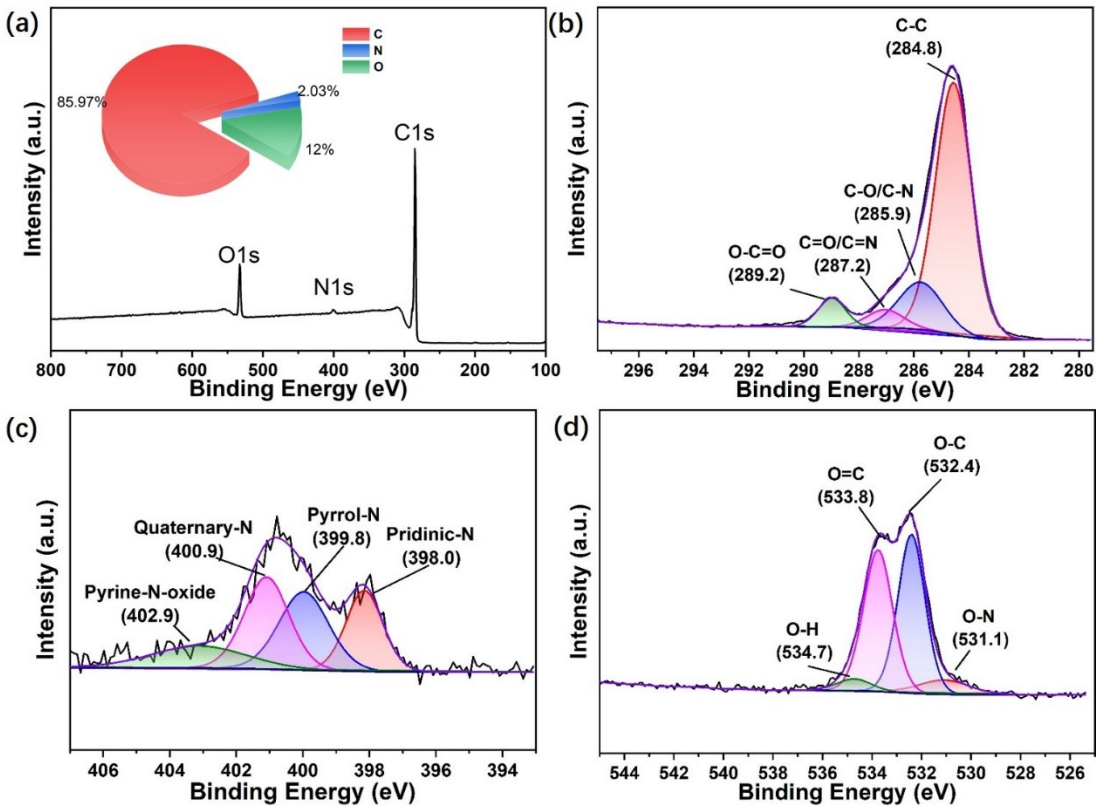


Fig. S4. (a) The XPS survey spectra, (b) high-resolution XPS C1s spectra, (c) high-resolution XPS N1s spectra, and (d) high-resolution XPS O1s spectra of NPCS-0.5.

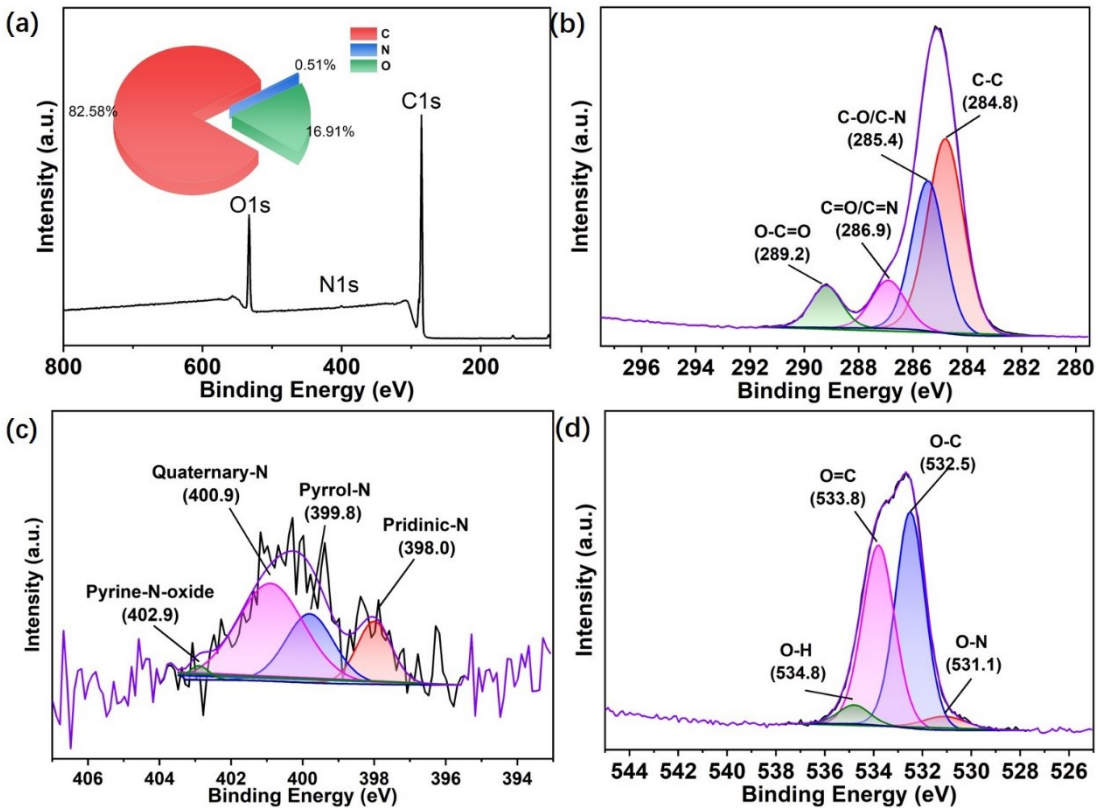


Fig. S5. (a) The XPS survey spectra, (b) high-resolution XPS C1s spectra, (c) high-resolution XPS N1s spectra, and (d) high-resolution XPS O1s spectra of NPCS-1.5.

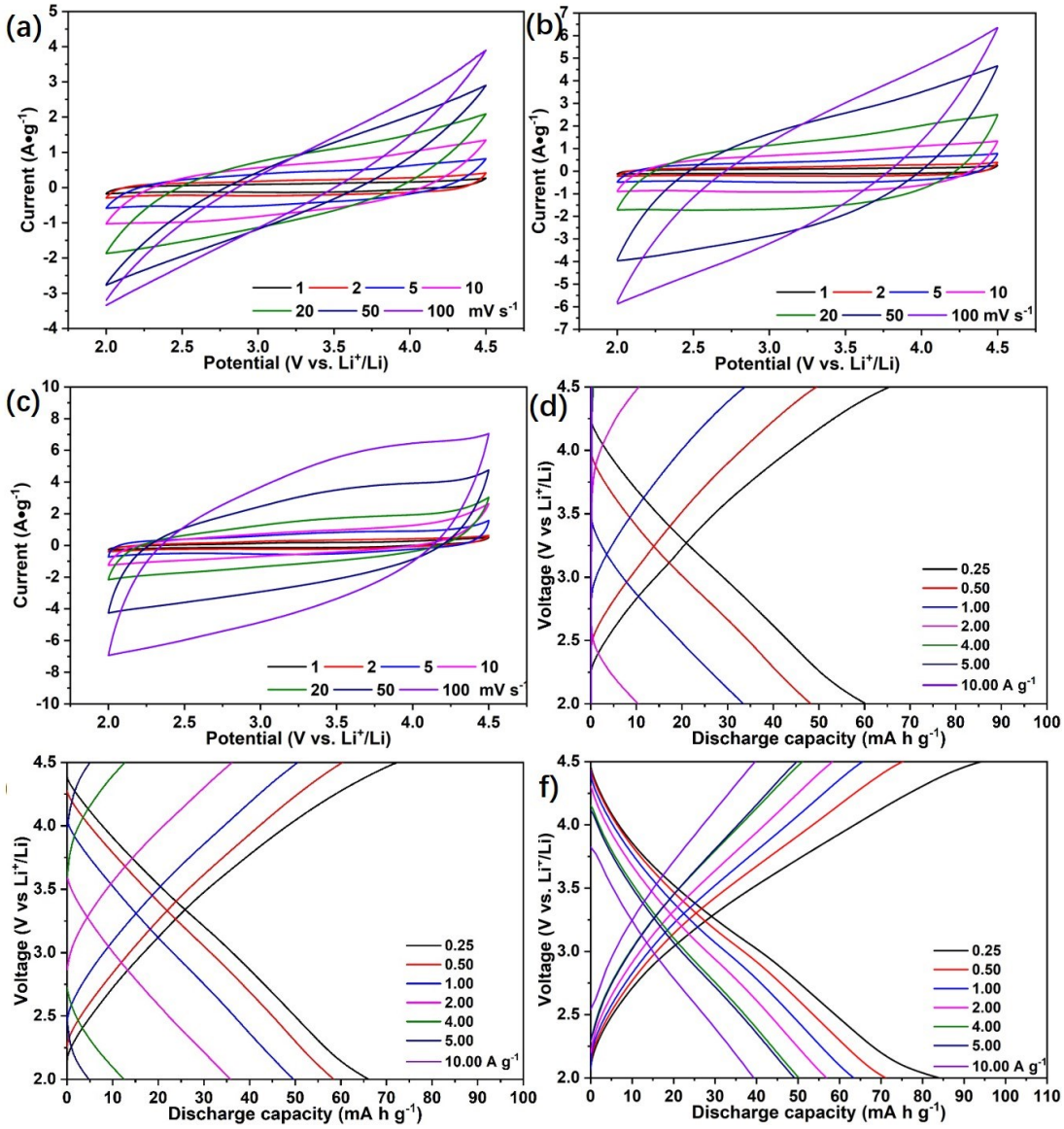


Fig. S6. CV curves of the NPCS-0 (a), NPCS-0.5 (b) and NPCS-1.5 (c) cathode at different scan rates; Charge–discharge curves of the NPCS-0 (d), NPCS-0.5 (e) and NPCS-1.5 (f) at different current densities.

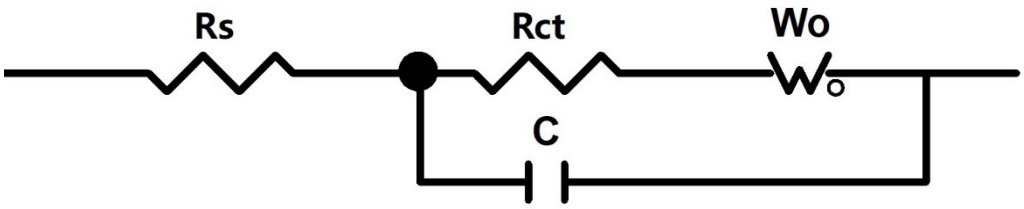


Fig. S7. The electrical equivalent circuit for the calculation of the resistances.

Table S1. Physical properties of NPCS-0, NPCS-0.5, NPCS-1 and NPCS-1.5.

| sample | yield g/g. % sugar | Specific Surface area $m^2/g$ | Total Pore Volume (ml/g) | Micropore Volume (ml/g) | N (wt.%) | C (wt.%) | H (wt.%) | Conductivity (s/cm) |
|---|---|---|---|---|---|---|---|---|
| NPCS-0 | 5.02 | 680.8 | 0.78 | 0.09 | 5.36 | 78.59 | 3.49 | 1.42 |
| NPCS-0.5 | 7.32 | 692.0 | 0.89 | 0.09 | 5.16 | 81.35 | 3.03 | 1.99 |
| NPCS-1 | 9.11 | 723.0 | 0.86 | 0.14 | 4.21 | 81.46 | 3.55 | 4.98 |
| NPCS-1.5 | 8.43 | 825.5 | 0.95 | 0.17 | 3.85 | 81.44 | 3.38 | 2.49 |

The specific surface area (SSA) was estimated by the Barrett−Emmett−Teller (BET) method. The total volume was estimated by the Barrett-Joyner-Halenda (BJH) method, based on the range of $P/P_0$ is 0.154 to 0.95. The micropore volume was analyzed using the density functional theory (DFT), based on the range of $P/P_0$ is 0 to 0.154.

Table S2. Relative surface concentrations of carbon, nitrogen, oxygen, carbon species, nitrogen species and oxygen species of NPCS-0, NPCS-0.5, NPCS-1, and NPCS-1.5.

| sample | Relative surface concentrations of atom | | | Relative surface concentrations of species | | | | | | | | | | |
|---|---|---|---|---|---|---|---|---|---|---|---|---|---|---|
| | C (at.%) | N (at.%) | O (at.%) | C=C/C-C (at.%) | C-N/C-O (at.%) | C=N/C=O (at.%) | O-C=O (at.%) | Pyridinic-N (at.%) | Pyrrolic-N (at.%) | Quaternary-N (at.%) | Pyrine-N-oxide (at.%) | O-N (at.%) | O-C (at.%) | O=C (at.%) | O-H (at.%) |
| NPCS-0 | 84.63 | 1.53 | 13.84 | 63.96 | 16.83 | 12.34 | 6.85 | 21.16 | 31.21 | 32.8 | 14.81 | 5.37 | 45.77 | 32.32 | 16.52 |
| NPCS-0.5 | 85.76 | 2.02 | 11.97 | 72.03 | 16.56 | 5.23 | 6.18 | 22.75 | 29.64 | 31.52 | 16.09 | 7.55 | 45.07 | 43.19 | 4.19 |
| NPCS-1 | 88.24 | 2.76 | 8.89 | 64.63 | 21.84 | 7.28 | 6.25 | 23.62 | 20.19 | 37.63 | 18.56 | 13.2 | 43.39 | 35.22 | 8.19 |
| NPCS-1.5 | 82.58 | 0.51 | 16.91 | 47.28 | 32.97 | 11.06 | 8.67 | 12.13 | 26.06 | 59.16 | 2.64 | 4.49 | 47.74 | 43.34 | 4.43 |

Table S3. Comparisons of the reported LIC systems with our NPCS-1//NPCS-1.

| LIC systems(anode//cathode) | Loading mass of active materials (mg $cm^{-2}$) | Electrolyte | Voltage window (V) | Energy density (Wh $kg^{-1}$) | Power density (W $kg^{-1}$) | Ref. |
|---|---|---|---|---|---|---|
| Hard carbon//activated carbon | 6.7 | 1.2 mol $L^{-1}$ $LiPF_6$ in EC:DEC (1:1 in volume) | 2.0 to 4.0 V | 83.4 | 800 | 9 |
| $Nb_2O_5$//activated carbon | 1.5 ~ 2.0 | 1.0 mol $L^{-1}$ $LiPF_6$ in EC:DMC (1:1 in volume) | 1.0 to 3.5 V | 65.39 | 5350.9 | 10 |
| Porous graphitic carbons//activated carbon | 0.7 ~ 0.9 | 1.0 mol $L^{-1}$ $LiPF_6$ in EC:DEC:DMC (1:1:1 in volume) | 2.0 to 4.0 V | 44.2 | 6527 | 11 |
| $Fe_3O_4$@reduced graphene oxide//activated carbon | / | 1.0 mol $L^{-1}$ $LiPF_6$ in EC:DEC:DMC (1:1:1 in volume) | 0.4 to 4.0 V | 98.8 | 343.8 | 12 |
| $V_2O_3$@carbon nanofibers//activated carbon | 1.1 | 1.0 mol $L^{-1}$ $LiPF_6$ in EC:DMC (1:1 in volume) | 0.0 to 4.0 V | 73.6 | 1000 | 13 |
| $MoS_2$@carbon//activated carbon | / | 1.0 mol $L^{-1}$ $LiPF_6$ in EC:DEC:DMC (1:1:1 in volume) | 0.0 to 4.5 V | 78.98 | 11250 | 14 |
| Graphene carbon//graphene-based porous carbon | 3.0 ~ 4.0 | 1.0 mol $L^{-1}$ $LiPF_6$ in EC:DEC:DMC (1:1:1 in volume) | 0.0 to 4.2 V | 50 | 12100 | 19 |
| N-rich boron carbonitride//B-rich boron carbonitride | 0.5 ~ 1.0 | 1.0 mol $L^{-1}$ $LiPF_6$ in EC:DMC (1:1 in volume) | 0.0 to 4.8 V | 160.3 | 1000 | 22 |
| $MnO_2$@graphene-like nanosheets//nanoporous carbon nanosheets | 1.5 ~ 2.0 | 1.0 mol $L^{-1}$ $LiPF_6$ in EC:DMC (1:1 in volume) | 0.0 to 4.0 V | 49.3 | 3900 | 24 |

| | | | | | | |
|---|---|---|---|---|---|---|
| Ni/NiO@carbon//N-doped MOF carbon | 1.6 ~ 2.4 | 1.0 mol $L^{-1}$ $LiPF_6$ in EC:DEC (1:1 in volume) | 0.0 to 4.0 V | 67 | 1000 | 25 |
| $MoS_2$@N-doped carbon//hierarchical porous carbon | 1.0 | 1.0 mol $L^{-1}$ $LiPF_6$ in EC:DEC:DMC (1:1:1 in volume) | 0.0 to 4.0 V | 47.4 | 10000 | 28 |
| N-doped carbon//N-doped carbon | / | 1.0 mol $L^{-1}$ $LiPF_6$ in EC:DMC (1:1 in volume) | 0.0 to 4.0 V | 116.9 | 500 | 29 |
| Graphite//B, N dual-doping carbon | / | 1.0 mol $L^{-1}$ $LiPF_6$ in EC:DEC:DMC (1:1:1 in volume) | 1.0 to 4.0 V | 114.2 | 250 | 30 |
| N doping carbon nanospheres //N doping carbon nanospheres | ~1.2 | 1.0 mol $L^{-1}$ $LiPF_6$ in EC:DEC (1:1 in volume) | 0.0 to 4.5 V | 206.7 | 225 | 32 |
| N, O co-doped porous carbon nanosheets// N, O co-doped porous carbon nanosheets | 1.0 ~ 2.0 | 1.0 mol $L^{-1}$ $LiPF_6$ in EC:DEC:DMC (1:1:1 in volume) | 0.0 to 4.0 V | 184 | 200 | 33 |
| Mesopore-dominant porous carbons//mesopore-dominant porous carbons | 2.0 | EMIM-$BF_4$ | 0.0 to 3.5 V | 109.9 | 4400 | 35 |
| High-defect porous carbon// high-defect porous carbon | 1.0 ~ 2.0 | 1.0 mol $L^{-1}$ $LiPF_6$ in EC:DEC:DMC (1:1:1 in volume) | 0.1 to 4.0 V | 106.4 | 500 | 36 |
| Hierarchical porous carbon //hierarchical porous carbon | / | 1.0 mol $L^{-1}$ $LiPF_6$ in EC:DEC:EMC (1:1:1 in volume) | 2.0 to 4.0 V | 97 | 55 | 38 |

| | | | | | | |
|---|---|---|---|---|---|---|
| NPCS-1//NPCS-1 | ~1.5 | 1.0 mol $L^{-1}$ $LiBF_4$ in EC:DEC:DMC (1:1:1 in volume) | 0.0 to 4.0 V | 135.6<br>69.0 | 500<br>10000 | This work |